Journal of Materials Chemistry C

PAPER

View Article Online
View Journal | View Issue

Cite this: J. Mater. Chem. C, 2015, 3, 4050

Sub-nanometer sized $Cu_6(GSH)_3$ clusters: one-step synthesis and electrochemical detection of glucose†

Xiaohui Gao,[ab] Yizhong Lu,[ab] Minmin Liu,[ab] Shuijian He[ab] and Wei Chen*[a]

Received 25th January 2015,
Accepted 6th March 2015

DOI: 10.1039/c5tc00246j

www.rsc.org/MaterialsC

We report here a one-pot synthesis of sub-nanometer sized copper clusters capped with a water-soluble ligand, L-glutathione (SGH), through a chemical reduction process. The composition of the as-prepared $Cu_6(SG)_3$ nanoclusters was confirmed by electrospray ionization mass spectrometry (ESI-MS) and matrix-assisted laser desorption ionization time-of-flight mass spectroscopy (MALDI-TOF MS). The FTIR, ^1H NMR and XPS characterization methods showed that with the production of $Cu_6(SG)_3$ clusters and the formation of Cu–S bonds, the surface chemical environment of the clusters exhibited a significant change. The produced water-soluble clusters show aggregation-induced fluorescence upon the addition of ethanol into the cluster aqueous solution. By loading on the TiO_2 support, the as-prepared copper nanoclusters were successfully applied to the electrochemical detection of glucose. Compared to large Cu nanoparticles, the $Cu_6(SG)_3$ nanoclusters exhibited higher sensitivity and a wider linear range for glucose detection.

1. Introduction

Noble metal nanoclusters consisting of several to hundreds of atoms have attracted intensive attention due to their size-dependent unique physical and chemical properties resulting from their discrete energy levels and band-gap energy structures, and their wide range of potential applications in biosensors, nanodevices, data storage, catalysis, *etc.*[1–6] In recent years, numerous efforts have been focused on the composition-controlled synthesis, structure-dependent properties and the practical applications of metal nanoclusters.[3,7–9] Although there are big challenges in investigating the nanoclusters with tiny core size, much progress has been achieved in this area, especially for gold and silver nanoclusters. Since the two-phase method was reported by Brust *et al.* for the preparation of monolayer-protected gold nanoparticles,[10] various strategies, such as modified Brust–Schiffrin methods, template-based synthesis, ligand-exchange reaction and electrochemical synthesis, have been developed for the synthesis of size-tunable metal nanoclusters.[3,11,12] In addition to gold and silver, the synthesis and properties of copper nanoclusters have also been investigated extensively recently.[13–16] Compared to the counterparts, *i.e.* Au and Ag, the low stability of Cu makes it more difficult to obtain tiny stable copper clusters. Up to now, by using various templates, DNA or organic molecules, stable copper nanoclusters have been successfully prepared. For example, blue emitting copper clusters have been synthesized in the presence of lysozyme.[17] The preparation of DNA-hosted copper nanoclusters has also been successfully realized.[16] In another study, copper quantum clusters were also produced by an electrochemical method and its polypyrrole film was used as a glutathione sensor.[18] To produce monolayer-protected copper clusters, it is important to find appropriate ligands which can well protect the copper core. As a kind of effective protecting ligand, glutathione (GSH) has been used to prepare metal nanoclusters.[19–21] Recently, Wang and co-workers synthesized monodisperse GSH-stabilized Cu nanoclusters through the so-called size-focusing etching process from Cu nanocrystals (~4.2 nm in diameter).[22] However, direct synthesis of GSH-stabilized Cu clusters with small size has not yet been reported. Based on the synthesis of gold and silver nanoclusters, we aim to here find a new strategy for the preparation of glutathione-stabilized copper nanoclusters and explore their application in analysis.

Due to the unique photoluminescence properties and high catalytic activities, metal nanoclusters have exhibited promising applications in many fields, such as chemical sensors, catalysis, biomedicine, *etc.*[23,24] When metal nanoclusters are used as catalysts, appropriate supports are usually needed to not only improve their dispersity but also enhance the stability. Among the materials, carbon and transition metal oxides are most widely

[a] State Key Laboratory of Electroanalytical Chemistry, Changchun Institute of Applied Chemistry, Chinese Academy of Sciences, Changchun 130022, Jilin, China. E-mail: weichen@ciac.ac.cn; Tel: +86 431 85262723
[b] University of Chinese Academy of Sciences, Beijing 100039, China

† Electronic supplementary information (ESI) available: Dependence of the fluorescence intensity of C-dots on the mixing time. See DOI: 10.1039/c5tc00246j

used as supports. For instance, carbon-supported Au_{25} clusters were used as catalysts for the reduction of 4-nitrophenol,[24] and CeO_2-surpported Au clusters were investigated for CO oxidation.[25] By taking advantage of the excellent electrocatalytic properties, copper nanoparticles and nanoclusters have been applied to the oxygen reduction reaction and non-enzyme electrochemical detection of glucose.[7,13]

Here, we developed a facile one-step method to prepare water-soluble Cu_6 nanoclusters (Cu NCs) by using L-glutathione (GSH) as the protecting ligand. The prepared nanoclusters exhibited aggregation-induced orange fluorescence in the mixed ethanol and water solution. By dispersing the as-prepared Cu clusters on the TiO_2 support, the resultant Cu NC/TiO_2 composites can be used to fabricate a non-enzymatic electrochemical sensor for sensitive and selective detection of glucose.

2. Experimental section

2.1 Materials

Copper dichloride dihydrate ($CuCl_2{\cdot}2H_2O$) was purchased from Tianjin Huadong Reagent. L-Glutathione (L-GSH) was obtained from Sigma-Aldrich. Hydrazine hydrate ($N_2H_4{\cdot}H_2O$) was obtained from Beijing Yili Chemical Co., Ltd. Sodium hydroxide (NaOH), titanium dioxide powder (TiO_2, with a diameter of 80 nm) and glucose ($C_6H_{12}O_6$) were bought from Beijing Chemical Reagent. All the reagents in this study were of analytical reagent grade and used as received. Water was supplied using a Water Purifier Ultrapure water system (18.3 MΩ cm)

2.2 Syntheses of Cu nanoclusters (Cu NCs) and the Cu NC/TiO_2 composites

The GS-protected Cu NCs were prepared by a one-pot method. Briefly, 2.5 ml of aqueous solution containing 21.5 mg of $CuCl_2{\cdot}2H_2O$ was added to the solution containing 76.5 mg of GSH under vigorous stirring. After the pH value dropped to 2–3, 250 μl, 50 mmol of sodium hydroxide solution was introduced into the reaction mixture with a slow stirring speed. After 10 min, 0.5 ml of hydrazine hydrate was then added dropwise to the mixture. The color of the solution turned from colorless to yellow-green, and then to gold yellow in half an hour. After three hours of stirring, the reaction flask was moved to the fridge and aged overnight in order to obtain stable Cu NCs. The finally obtained nanoclusters were purified by adding ethanol in the cyclic method of precipitation and centrifugation and dissolved in water for further use.

Cu NC/TiO_2 composites were synthesized by a simple implantation process. Typically, 2 mg of TiO_2 powder was dispersed in 1 ml of water under ultrasound and then mixed with 0.5 ml of 17 mg ml^{-1} Cu NC aqueous solution under vigorous stirring for 20 h at room temperature. The resultant precipitate was collected by centrifugation and dispersed in water for further use. The color of the obtained Cu NC/TiO_2 composites is obviously different from that of the pure TiO_2, suggesting the successful dispersion of the Cu NCs on the TiO_2 support.

2.3 Syntheses of Cu nanoparticles (Cu NPs) and the Cu NP/TiO_2 composites

The large GSH-protected Cu NPs were synthesized following the above procedure of preparing Cu NCs with some modification. In brief, 2.5 ml of 42.0 mg $CuCl_2{\cdot}2H_2O$ in aqueous solution was introduced into a flask containing 20 mg of glutathione and 2.5 ml of water. After 30 min, 1 ml of ethanol and 60 mg of solid $NaBH_4$ were added into the above mixture successively. The reaction was allowed to continue for 4 h at room temperature. Finally, the ethanol–water solvent mixture was used to wash and collect the Cu NPs. The preparation of Cu NP/TiO_2 composites is similar to that of Cu NC/TiO_2 composites, just by replacing Cu NCs with Cu NPs.

2.4 Material characterization

UV-Vis spectra were recorded on a UV-3000PC spectrophotometer (Shanghai Manada Instrmenta Co., Ltd). Photoluminescence spectra were recorded on a Perkin-Elmer LS-55 Luminescence spectrometer (Perkin-Elmer Instruments UK). X-Ray photoelectron spectroscopy (XPS) measurements were performed by using an AVG Thermo ESCALAB 250 spectrometer (VG scientific) operated at 120 W. Matrix-assisted laser-desorption ionization time of flight mass spectrometric (MALDI-TOF MS) studies were performed using a Bruker autoflexIII smartbeam MALDI-TOF/TOF-MS (Germany) and 2,5-dihydroxy benzoic acid (DHB) was used as the matrix. Electrospray ionization mass spectrometry (ESI-MS) measurements were conducted on a LTQ linear ion trap mass spectrometer (Thermo, San Jose, CA, USA), equipped with a conventional ESI source. ESI-MS spectra in both negative- and positive-modes were collected. Fourier-transform infrared spectroscopy (FTIR) study was conducted using a VERTTEX 70 FTIR (KBr wafer technique). ^{1}H NMR was carried out by using an Avance III HD 500 (Switzerland, Bruker).

2.5 Polyacrylamide gel electrophoresis (PAGE)

The polyarylamide gel electrophoresis experiment was performed following the previous report with a little modification.[20] Homemade gels were prepared with 30% concentration of acrylamide monomer and 4% bis-acrylamide cross-linker for the resolving gel. The stacking gel was made with 4% monomer concentration. The gel dimensions were 20 cm × 20 cm × 1.5 mm. THAM (25 mM) and glycine (192 mM) were used as the eluting buffers. In the stacking gel, the voltage was set at 80 V, and in the resolving gel, the voltage was set at 120 V. All processes were conducted at room temperature.

2.6 Thin layer chromatography (TLC)

The TLC process was performed at room temperature. Ethanol and water with different volume ratios were used as mobile phases, including ethanol : water = 1 : 10, 1 : 9, 1 : 8, 1 : 6, 1 : 1, 1 : 2, 5 : 1, 5 : 2, 2 : 3, 1 : 0, and 0 : 1. The results obtained from the different mobile phases are almost the same.

2.7 Electrochemical measurements

A piece of ITO substrate was cleaned first by water, acetone and ethanol in an ultrasound bath and was dried at room temperature.

The mixture of the Cu NC/TiO_2 composites or TiO_2 dispersing solution and 0.5% of Nafion solution was then dropcast onto the clean ITO substrate and dried at ambient temperature. Control experiments were also performed on blank ITO, ITO modified with only TiO_2, and the Cu NP/TiO_2 composites. The electrodes were denoted as Cu NC/TiO_2/ITO, ITO, TiO_2/ITO, and Cu NC/TiO_2/ITO, respectively. The geometric areas were measured to be 0.7, 0.8, 0.8, and 1.0 cm^2 for pure ITO, CuNC/TiO_2/ITO, TiO_2/ITO and CuNP/TiO_2/ITO electrodes, respectively.

Electrochemical measurements, including cyclic voltammograms and amperometric response, were carried out using a CHI 750D electrochemical workstation in a standard three-electrode cell at room temperature. The ITO, TiO_2/ITO, CuNC/TiO_2/ITO and CuNP/TiO_2/ITO electrodes prepared above were used as working electrodes. An Ag/AgCl (in 3 M NaCl, aq.) and a Pt coil were used as reference and counter electrodes, respectively. All the electrochemical measurements were performed in 0.1 M KOH solution and at room temperature.

2.8 Catalytic reaction of the methylene blue (MB) to leucomethylene blue (LMB)

The catalytic reduction reaction was performed following the reported procedure.[26,27] Typically, under magnetic stirring, 100 μl of 8 mg ml^{-1} Cu NC solution was introduced into 2.9 ml aqueous solution with 33 μM MB and 60 mM N_2H_4. The UV-Vis absorption spectra of the solution before and after catalytic reaction were collected for comparison.

3. Results and discussion

3.1 Synthesis and characterization of Cu nanoclusters

Compared to the recent two-step preparation,[22] we present here a one-step method to synthesize Cu_6 nanoclusters without the etching step. In the present preparation, upon addition of $CuCl_2$ into the GSH aqueous solution, transparent Cu(I)–GS micelles can be formed gradually, which is likely to be the intermediates of Cu NCs. The addition of NaOH could improve the stability of the micelles and promote the growth of specific nanoclusters by changing the pH of the mixture. On the other hand, in order to control the reaction kinetics, a mild reducing reagent, $N_2H_4{\cdot}H_2O$, was chosen for the reduction of Cu(I) to Cu(0) to form Cu clusters. The as-synthesized Cu nanoclusters are very stable at room temperature. Fig. S1 (ESI†) displays the solution and solid forms of the as-synthesized copper nanoclusters.

The exact size of metal nanoclusters can be hardly resolved by TEM measurements because of their tiny core size. However, it is well-known that mass spectroscopy is a powerful technique to identify the composition and the exact atom numbers of metal nanoclusters. Here, the core size and the composition of the as-synthesized Cu clusters were first characterized by matrix-assisted laser desorption ionization time-of-flight mass spectroscopy (MALDI-TOF MS) measurements. Fig. 1A shows the full MALDI-TOF mass spectrum of the as-prepared Cu NCs. The highest mass peak can be observed at *m/z* 737.01, which is ascribed to $[Cu_2(SG)_2–H]^-$. Another pronounced peak at *m/z*

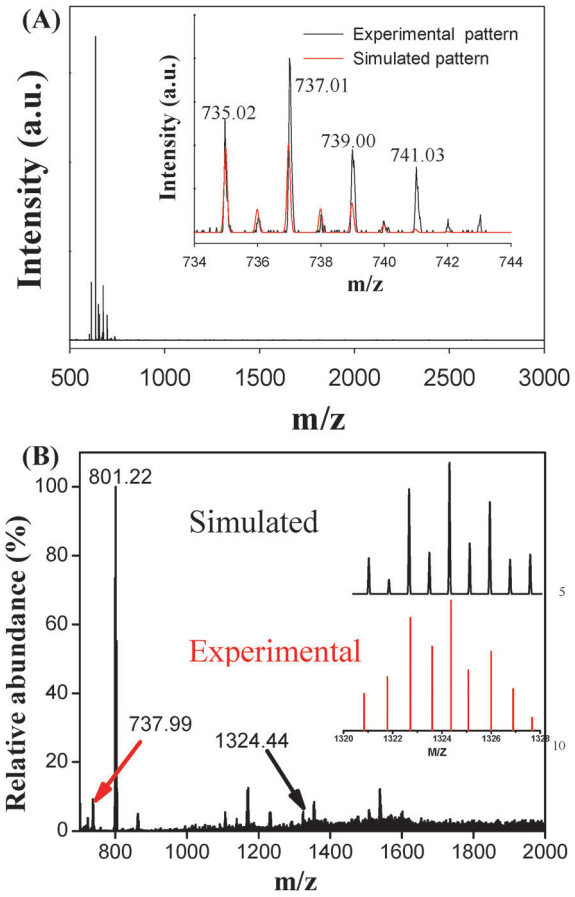

Fig. 1 (A) The negative-mode MADLI-TOF MS of the as-synthesized Cu nanoclusters. The inset shows the experimental (black curve) and simulated (red curve) isotopic patterns of $[Cu_2(SG)_2–H]^-$. (B) The positive-mode ESI-MS of the as-synthesized Cu nanoclusters. The inset shows the experimental (red curve) and simulated (black curve) isotopic patterns of $[Cu_6(SG)_3 + H + Na]^+$.

675.03 could be assigned to the $[Cu(SG)_2]^-$ fragments. Fig. 1A (inset) and Fig. S2 (ESI†) show the experimental and simulated isotopic patterns of the $[Cu_2(SG)_2–H]^-$ and $[Cu(SG)_2]^-$, respectively. The high consistency between the experimental and simulated data indicates the successful synthesis of copper clusters. However, during the MALDI-TOF MS analysis, the highly energetic ionization process may lead to the formation of fragments. That is to say the $[Cu_2(SG)_2]^-$ may be the fragments from larger nanoclusters. Therefore, a softer mass spectrometry, electrospray ionization mass spectrometry (ESI-MS), was also performed to further analyze the composition of the formed Cu clusters. As shown in Fig. 1B, positive-mode ES-MS analysis gives obvious isotope features of copper, and the peak at *m/z* 1324.44 indicates the $Cu_6(GS)_3$ composition of the original Cu NCs. It can be seen from Fig. 1B (inset) that the experimental pattern has a good match with the simulated spectra. It is noteworthy that the most abundant peak located at *m/z* 801.22 could be assigned to the fragment of $[Cu_3(SG)_2]^+$. The experimental and stimulated isotopic patterns of $[Cu_3(SG)_2]^+$ are compared in Fig. S3 (ESI†). Interestingly, the isotopic peak centered at *m/z* 737.99 from $[Cu_2(SG)_2 + H]^+$ also appears in ESI-MS, which is consistent with the result from

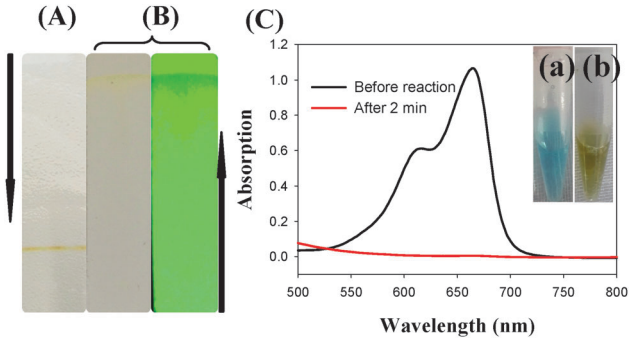

Fig. 2 (A) Polyacrylamide gel electrophoresis (PAGE) results and (B) thin layer chromatography (TLC) results (left: under sunlight; and right: under ultra-violet light) of the as-synthesized Cu cluster. (C) UV-Vis absorption spectra of the mixture of MB and N_2H_4 before and after the addition of Cu NCs. The inset shows digital photographs of the mixed solution before (a) and after 2 min (b) reaction with Cu NCs.

MALDI-TOF MS. Such results suggest that $[Cu_2(SG)_2]^-$ is indeed from the as-prepared $Cu_6(SG)_3$ clusters. In order to further characterize the as-synthesized Cu NCs, negative-mode ESI-MS was also performed, as displayed in Fig. S4 (ESI†). Surprisingly, we can also see the peak at *m*/*z* 800.98 from $[Cu_3(SG)_2–H]^-$, suggesting that $Cu_3(SG)_2$ may be the solid part of the parent cluster just like the "staple" motif $Au_x(SR)_y$ in Au clusters.[28–31] In the higher mass region, a fragment peak at *m*/*z* 1037.43 attributes to $[Cu_6(SG)_2 + 2Na]^-$, while in the lower mass region another fragment peak at 368.09 could be from $[Cu(SG)–H]^-$. Fig. S5 and S6 (ESI†) show their experimental and simulated isotopic patterns, respectively.

Polyacrylamide gel electrophoresis (PAGE) has been widely used to separate metal nanoclusters and analyze their dispersity.[12,20,32–34] As presented in Fig. 2A, after washing and centrifuging with the mixture of water and ethanol, the obtained clusters show only one yellow band in PAGE, indicating the high size homogeneity of the produced copper nanoclusters. On the other hand, thin layer chromatography (TLC) was conducted for the Cu clusters with varying volume ratios of ethanol–water mobile phases. As shown in Fig. 2B, only one yellow band can be observed, which is consistent with that of PAGE results. It is worthy to note that the TLC plate even doesn't show other obvious dots or bands under ultraviolet light. The appearance of only one yellow band in PAGE and TLC measurements also supports the above MS results, *i.e.* the as-prepared Cu cluster has the composition of $Cu_6(SG)_3$. On the other hand, Cu clusters with size less than 20 copper atoms are expected to exhibit catalytic activity for the reduction of methylene blue (MB) to leucomethylene blue (LMB) in the presence of hydrazine.[26] Fig. 2C shows the UV-Vis absorption spectra of MB solution before and after adding Cu nanoclusters. Upon the addition of the as-prepared $Cu_6(SG)_3$ clusters into the MB solution, the absorption between 500 and 800 nm from MB disappeared after 2 min. Fig. 2C (inset) shows that the original blue color of MB faded within two minutes. Such catalytic reaction further suggests the formation of small Cu nanoclusters.

To analyze the surface chemical bonding of the Cu NCs, Fourier transform infrared spectroscopy (FT-IR) and proton

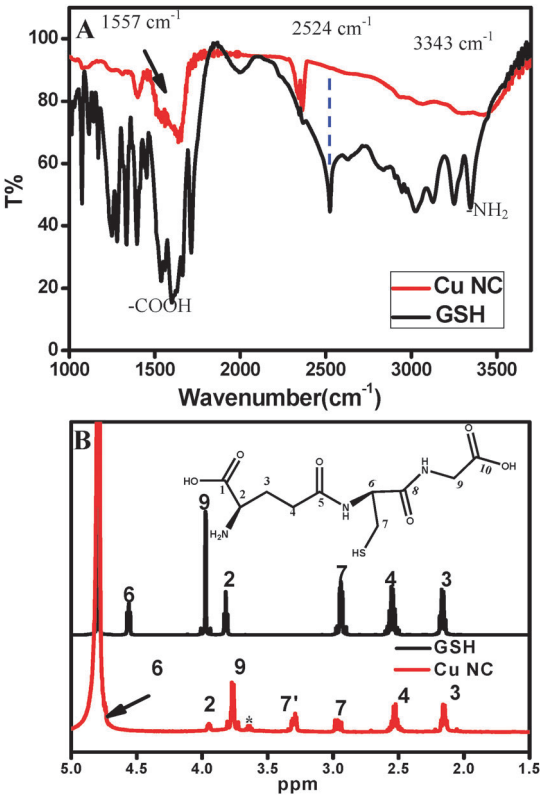

Fig. 3 FT-IR (A) and ^{1}H NMR (B) spectra of the glutathione ligand (black curve) and the as-synthesized $Cu_6(SG)_3$ nanoclusters (red curve). The inset of (B) shows the molecular structure of the glutathione ligand.

nuclear magnetic resonance (^{1}H-NMR) measurements were performed. Fig. 3A shows the FTIR spectra of free GSH ligands and the $Cu_6(SG)_3$ clusters. Compared to the spectrum of pure GSH ligands, the peak at 2524 cm^{-1} from –S–H stretching vibration disappears in the spectrum of Cu_6 clusters, while peaks located at 3343 and 1557 cm^{-1} that stem from $–NH_2$ and –COOH groups can still be observed. These results indicate that glutathione ligands have been successfully bound onto the surface of Cu_6 clusters through –S–Cu chemical bonds, with the cleavage of the S–H bond. Fig. 3B shows the ^{1}H NMR spectra of pure glutathione and $Cu_6(SG)_3$ in the range of 1.5 to 5.0 ppm. Based on the molecular structure of glutathione shown in Fig. 3B (inset) and the previous reports, the observed NMR peaks from different protons have been assigned (labeled with carbon numbers).[20,35] The strong peaks at 4.79 ppm attribute to D_2O and the weak peak at 3.56 ppm (marked with asterisk) could be ascribed to the residual ethanol during cluster purification. All the rest of the peaks arise from free GSH or GSH capped on the surface of Cu NCs. Based on the chemical shifts, the signals at 2.16 and 2.54 ppm could be easily assigned to the protons on C3 and C4. Interestingly, it can be seen that the peak from C7 splits into two peaks in the spectrum of Cu_6–GSH clusters (labeled with 7 and 7′ in Fig. 3B). According to the previous study,[35] such splitting is caused by the adjacent chiral carbon (C6). It should be noted that because C6 and C7 are very close to the copper cores, the

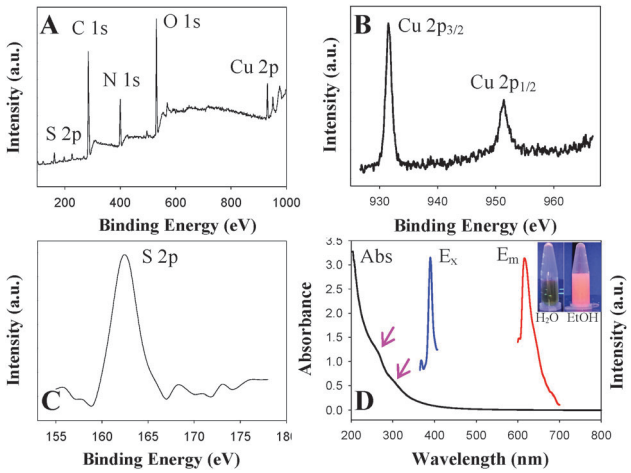

Fig. 4 (A) XPS survey spectrum of the Cu nanoclusters. XPS spectra of Cu 2p (B) and S 2p (C) of Cu nanoclusters. (D) UV-Vis absorption (black curve), photoluminescence excitation (blue curve, λ_{em} = 617 nm) and emission (red curve, λ_{ex} = 390 nm) spectra of the as-synthesized Cu NCs. The absorption was measured in aqueous solution; the excitation and emission spectra were collected in the mixture of water and ethanol (~80 vol%). The inset shows the photographs of the Cu NCs in aqueous solution (left) and the mixed solution (right) under UV light.

corresponding proton signals usually have downfield shifts. Therefore, the proton signals from C6 may merge in the strong water peak in the ^{1}H-NMR spectrum, as shown in Fig. 3B. These ^{1}H NMR features further suggest the formation of GSH-protected copper nanoclusters.[36–40]

X-ray photoelectron spectroscopy (XPS) analysis was also utilized to characterize the oxidation state of the Cu nanoclusters. The XPS survey spectrum shown in Fig. 4A indicates the presence of Cu, C, N, and S in the product. Fig. 4B shows the Cu 2p XPS spectrum, in which the peaks at 951.5 and 931.5 eV can be assigned to the binding energies of Cu $2p_{1/2}$ and Cu $2p_{3/2}$ from Cu(0). As described before,[13] due to the indiscernible binding energies (~0.1 eV difference) of Cu(0) and Cu(I) and the possible charge transfer in the Cu–SR bonds, the oxidation states of the prepared Cu NC may involve 0 and +1. It should be pointed out that the binding energy of Cu^{2+} around 942 eV was not observed in the Cu 2p spectrum (Fig. 4B), indicating the formation of pure metallic copper clusters. The S 2p peak corresponds to the binding energy of chemisorbed sulfur (Fig. 4C). The XPS spectra of C and N are displayed in Fig. S7 (ESI†). Fig. 4D shows the UV-Vis absorption of the obtained Cu NCs in water (black curve). The two broad absorption bands at around 260 and 305 nm may correspond to the interband transition. Moreover, the surface plasmonic resonance (SPR) of Cu nanocrystals (~570 nm) does not appear in the UV-Vis spectrum. The step-like feature and the absence of SPR absorption further confirm the successful preparation of molecule-like Cu NCs. Photoluminescence is another intriguing characteristic of metal nanoclusters. Interestingly, the as-synthesized Cu_6 nanoclusters showed very weak fluorescence in water. However, upon addition of ethanol into the cluster aqueous solution, strong orange emission can be observed. As shown in Fig. 4D and the inset, under UV irradiation, the Cu_6 nanoclusters in the mixed solution (~80 vol% ethanol) exhibit intense emission at 617 nm. As reported previously,[41] such a result indicates the obvious aggregation-induced emission (AIE) enhancement effect of the Cu_6 nanoclusters. Similar to the AIE of gold clusters, the observed enhanced fluorescence of the present clusters is probably from the AIE of Cu(I)–thiolate complex on the cluster surface.

3.2 Non-enzymatic electrochemical detection of glucose with the Cu_6 nanoclusters

The electrocatalytic activity of the Cu NCs for glucose oxidation and the application in non-enzymatic glucose detection were studied by electrochemistry. Here, in order to enhance the dispersity of Cu NCs and to avoid the degradation and aggregation of Cu NCs in electrochemical measurements, TiO_2 powder was used as the Cu NC catalyst support. After 20 h stirring of the mixture, the color of TiO_2 changed from white to orange, suggesting the successful loading of Cu NCs on the TiO_2 support. For comparison, large Cu nanoparticles (Cu NPs) with an average size of 157.4 ± 3.4 nm (DLS data are shown in Fig. S8, ESI†) were also prepared and their electrocatalytic activity was studied by loading on TiO_2. Fig. 5A shows the cyclic voltammograms (CVs) of different electrodes in 0.1 M KOH with the presence of 5 mM glucose. Clearly, almost no oxidation current can be observed from the pure ITO and TiO_2/ITO electrodes, indicating the poor electrocatalytic activities of ITO and TiO_2 for glucose oxidation. However, under the same conditions, large oxidation current density was obtained on the Cu NC/TiO_2/ITO electrode. By comparison, the current density obtained from Cu NC/TiO_2/ITO is much higher than that of

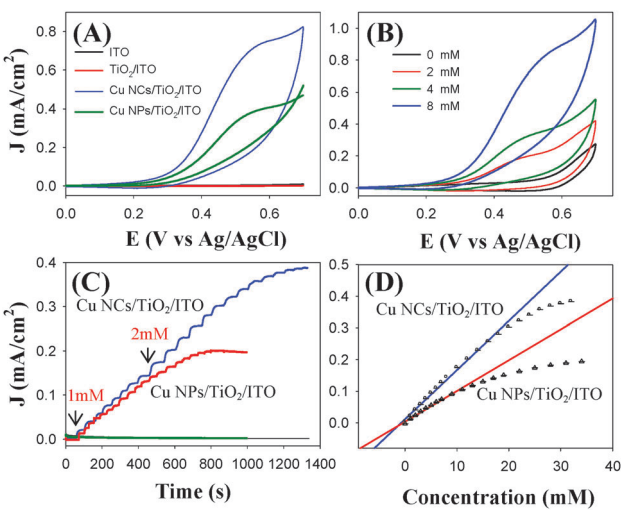

Fig. 5 (A) Cyclic voltammograms (CVs) of ITO (black line), TiO_2/ITO (red line), Cu NC/TiO_2/ITO (blue line) and Cu NP/TiO_2/ITO (dark green line) in 0.1 M KOH with 5 mM glucose. Potential scan rate: 0.1 V s^{-1}. (B) CVs of Cu NC/TiO_2/ITO in 0.1 M KOH with different concentrations of glucose (0, 2, 4, and 8 mM). Potential scan rate: 0.1 V s^{-1}. (C) Aperometric responses of Cu NC/TiO_2/ITO and Cu NP/TiO_2/ITO to glucose at 0.5 V in 0.1 M KOH; the black and dark green lines show the J–t curves with the absence of glucose in the electrolyte. (D) The relationship of current density and concentration of glucose on the Cu NC/TiO_2/ITO and Cu NP/TiO_2/ITO electrodes, respectively.

Cu NP/TiO_2/ITO. Moreover, the onset potential of glucose oxidation on the present Cu NC/TiO_2/ITO (0.02 V) is more negative than that on Cu NP/TiO_2/ITO (0.09 V) and the previously reported Cu nanoparticles loaded on the graphene support.[7] Such CV comparison strongly demonstrates that the as-synthesized copper nanoclusters have enhanced catalytic activity for glucose oxidation. In order to study the sensitivity of the Cu NCs to the glucose concentration, the CVs of Cu NC/TiO_2/ITO in the electrolyte with different concentrations of glucose were recorded. As shown in Fig. 5B, the oxidation current density increases gradually with the concentration of glucose increasing from 0 to 8 mM. The CV studies indicate that the as-prepared Cu_6 nanoclusters could be used for the non-enzymatic electrochemical detection of glucose.

Fig. 5C presents the amperometric responses of the Cu NC/TiO_2/ITO and Cu NP/TiO_2/ITO electrodes against the glucose concentration. At the Cu NC/TiO_2/ITO electrode (blue curve), with a successive addition of glucose into the 0.1 M KOH electrolyte at +0.5 V, the oxidation current density continuously increases until the glucose concentration reaches 32 mM after which steady-state current density appears. The black baseline in Fig. 5C demonstrates that with the absence of glucose in the electrolyte, the Cu NC/TiO_2/ITO electrode can only give low and almost constant current density during the whole tested time (1400 s), which again confirms that the current responses are from the glucose oxidation on the Cu NCs. Similarly, Cu NP/TiO_2/ITO (red curve) also shows amperometric response to the glucose concentration, but with much lower sensitivity compared to the Cu NCs. The linear relationships (J–c curves) between the current density (J) and the glucose concentration (c) on the Cu NC/TiO_2/ITO and Cu NP/TiO_2/ITO electrodes are presented in Fig. 5D. From the fitting line obtained from the Cu NC/TiO_2/ITO electrode, the linear range locates between 4.07 μM and 20 mM, which is much wider than those obtained from the Cu_2O and Cu nanomaterials reported in the literature.[7,42,43] The linear calibration equation can be expressed as: $J = 0.0151 \times C + 0.0145$ and the limit of detection is evaluated to be 4.07 μM based on the equation of LOD = $3\sigma/s_d$. Here, s_d is the slope of the current–concentration curve and σ is the standard deviation of any five current points without the presence of glucose in the electrolyte. Meanwhile, from Fig. 5D, a linear calibration equation of $J = 0.0113 \times C + 0.0021$ with a linear range of 0–13 mM and an LOD of 13.6 μM were obtained from the Cu NP/TiO_2/ITO electrode. Obviously, the Cu NP/TiO_2/ITO electrode exhibits much lower sensing sensitivity and a narrower linear range compared to the Cu NCs. Based on these electrochemical results, it can be seen that the Cu_6 clusters exhibit much higher sensing performance than large Cu nanoparticles. Such size-dependent electrocatalytic activities of metal nanoclusters have also been observed before.[23,44,45] As is known, ascorbic acid (AA), dopamine (DA) and uric acid (UA) generally co-exist with glucose in human serum. The effects of these analytes on the glucose detection were also investigated. Fig. S9 and S10 (ESI†) show the amperometric responses upon addition of different analytes in 0.1 M KOH at 0.5 V. It should be noted the normal physical level of the above analytes is only 1/4–1/6 of glucose.[42] Here, much higher concentration of the analytes (10 mM) than that reported previously was used in the measurements. It can be seen that 10 mM NaCl and UA have little effect on the current response, while much lower current responses were obtained from 10 mM ascorbic acid and dopamine compared to that from glucose oxidation. The results indicate the high selectivity of the Cu_6 nanoclusters to the electrochemical detection of glucose.

4. Conclusion

In summary, GSH-protected Cu_6 nanoclusters were synthesized successfully by a one-step method. ESI-MS and MALDI-TOF MS measurements confirmed the $Cu_6(SG)_3$ composition of the formed nanoclusters. FTIR, ^{1}H NMR and XPS characterization methods showed the surface bonding of Cu–S and the metallic state of Cu. Moreover, the prepared Cu nanoclusters exhibited the aggregation-induced emission enhancement effect. By loading the Cu NCs on the TiO_2 support, the resultant composites can be used as novel electrochemical sensing materials for glucose detection. The sensor based on Cu_6 nanoclusters displayed a wider linear range and higher detection sensitivity compared with large Cu nanoparticles. We hope this work could open up a new route for the synthesis of Cu nanoclusters and provide a new application of Cu nanoclusters.

Acknowledgements

This work was supported by the National Natural Science Foundation of China (No. 21275136) and the Natural Science Foundation of Jilin province, China (No. 201215090).

Notes and references

1 R. C. Jin, *Nanoscale*, 2010, **2**, 343–362.
2 J. Zheng, P. R. Nicovich and R. M. Dickson, *Annu. Rev. Phys. Chem.*, 2007, **58**, 409–431.
3 Y. Z. Lu and W. Chen, *Chem. Soc. Rev.*, 2012, **41**, 3594–3623.
4 W. Chen and S. Chen, *Functional nanometer-sized clusters of transition metals: synthesis, properties and applications*, Royal Society of Chemistry, Cambridge, 2014.
5 Y. Z. Lu, Y. Y. Jiang, X. H. Gao and W. Chen, *Chem. Commun.*, 2014, **50**, 8464–8467.
6 M. M. Liu and W. Chen, *Nanoscale*, 2013, **5**, 12558–12564.
7 J. Luo, S. S. Jiang, H. Y. Zhang, J. Q. Jiang and X. Y. Liu, *Anal. Chim. Acta*, 2012, **709**, 47–53.
8 R. Z. Zhang and W. Chen, *J. Mater. Chem. A*, 2013, **1**, 11457–11464.
9 J. Ju and W. Chen, *Anal. Chem.*, 2015, **87**, 1903–1910.
10 M. Brust, M. Walker, D. Bethell, D. J. Schiffrin and R. Whyman, *J. Chem. Soc., Chem. Commun.*, 1994, 801–802.
11 X. Yuan, Z. T. Luo, Q. B. Zhang, X. H. Zhang, Y. G. Zheng, J. Y. Lee and J. P. Xie, *ACS Nano*, 2011, **5**, 8800–8808.
12 T. U. B. Rao, B. Nataraju and T. Pradeep, *J. Am. Chem. Soc.*, 2010, **132**, 16304–16307.

13 W. T. Wei, Y. Z. Lu, W. Chen and S. W. Chen, *J. Am. Chem. Soc.*, 2011, **133**, 2060–2063.
14 Y. Z. Lu, W. T. Wei and W. Chen, *Chin. Sci. Bull.*, 2012, **57**, 41–47.
15 H. Kawasaki, Y. Kosaka, Y. Myoujin, T. Narushima, T. Yonezawa and R. Arakawa, *Chem. Commun.*, 2011, **47**, 7740–7742.
16 X. F. Jia, J. Li, L. Han, J. T. Ren, X. Yang and E. K. Wang, *ACS Nano*, 2012, **6**, 3311–3317.
17 R. Ghosh, A. K. Sahoo, S. S. Ghosh, A. Paul and A. Chattopadhyay, *ACS Appl. Mater. Interfaces*, 2014, **6**, 3822–3828.
18 V. Saumya and T. P. Rao, *Anal. Methods*, 2012, **4**, 1976–1982.
19 Y. Yu, Z. T. Luo, D. M. Chevrier, D. T. Leong, P. Zhang, D. E. Jiang and J. P. Xie, *J. Am. Chem. Soc.*, 2014, **136**, 1246–1249.
20 S. Kumar, M. D. Bolan and T. P. Bigioni, *J. Am. Chem. Soc.*, 2010, **132**, 13141–13143.
21 X. D. Zhang, Z. T. Luo, J. Chen, X. Shen, S. S. Song, Y. M. Sun, S. J. Fan, F. Y. Fan, D. T. Leong and J. P. Xie, *Adv. Mater.*, 2014, **26**, 4565–4568.
22 X. F. Jia, J. Li and E. K. Wang, *Small*, 2013, **9**, 3873–3879.
23 W. Chen and S. W. Chen, *Angew. Chem., Int. Ed.*, 2009, **48**, 4386–4389.
24 A. Shivhare, D. M. Chevrier, R. W. Purves and R. W. J. Scott, *J. Phys. Chem. C*, 2013, **117**, 20007–20016.
25 Z. Wu, D.-E. Jiang, A. K. P. Mann, D. R. Mullins, Z.-A. Qiao, L. F. Allard, C. Zeng, R. Jin and S. H. Overbury, *J. Am. Chem. Soc.*, 2014, **136**, 6111–6122.
26 N. Vilar-Vidal, J. Rivas and M. A. Lopez-Quintela, *ACS Catal.*, 2012, **2**, 1693–1697.
27 X. F. Jia, X. A. Yang, J. Li, D. Y. Liab and E. K. Wang, *Chem. Commun.*, 2014, **50**, 237–239.
28 M. Zhu, C. M. Aikens, F. J. Hollander, G. C. Schatz and R. Jin, *J. Am. Chem. Soc.*, 2008, **130**, 5883–5885.
29 A. Das, C. Liu, C. J. Zeng, G. Li, T. Li, N. L. Rosi and R. C. Jin, *J. Phys. Chem. A*, 2014, **118**, 8264–8269.
30 T. W. Ni, M. A. Tofanelli, B. D. Phillips and C. J. Ackerson, *Inorg. Chem.*, 2014, **53**, 6500–6502.
31 C. L. Heinecke, T. W. Ni, S. Malola, V. Makinen, O. A. Wong, H. Hakkinen and C. J. Ackerson, *J. Am. Chem. Soc.*, 2012, **134**, 13316–13322.
32 L. M. Tvedte and C. J. Ackerson, *J. Phys. Chem. A*, 2014, **118**, 8124–8128.
33 Y. Shichibu, Y. Negishi, T. Tsukuda and T. Teranishi, *J. Am. Chem. Soc.*, 2005, **127**, 13464–13465.
34 Y. Shichibu, Y. Negishi, H. Tsunoyama, M. Kanehara, T. Teranishi and T. Tsukuda, *Small*, 2007, **3**, 835–839.
35 Z. W. Wu, C. Gayathri, R. R. Gil and R. C. Jin, *J. Am. Chem. Soc.*, 2009, **131**, 6535–6542.
36 D. Gentili, G. Ori and M. C. Franchini, *Chem. Commun.*, 2009, 5874–5876.
37 J. S. Seo, D. M. Son, H. Lee, J. Kim and Y. Kim, *Bull. Korean Chem. Soc.*, 2009, **30**, 2651–2654.
38 M. Cargnello, N. L. Wieder, P. Canton, T. Montini, G. Giambastiani, A. Benedetti, R. J. Gorte and P. Fornasiero, *Chem. Mater.*, 2011, **23**, 3961–3969.
39 R. H. Terrill, T. A. Postlethwaite, C. H. Chen, C. D. Poon, A. Terzis, A. D. Chen, J. E. Hutchison, M. R. Clark, G. Wignall, J. D. Londono, R. Superfine, M. Falvo, C. S. Johnson, E. T. Samulski and R. W. Murray, *J. Am. Chem. Soc.*, 1995, **117**, 12537–12548.
40 M. J. Hostetler, J. E. Wingate, C. J. Zhong, J. E. Harris, R. W. Vachet, M. R. Clark, J. D. Londono, S. J. Green, J. J. Stokes, G. D. Wignall, G. L. Glish, M. D. Porter, N. D. Evans and R. W. Murray, *Langmuir*, 1998, **14**, 17–30.
41 Z. T. Luo, X. Yuan, Y. Yu, Q. B. Zhang, D. T. Leong, J. Y. Lee and J. P. Xie, *J. Am. Chem. Soc.*, 2012, **134**, 16662–16670.
42 M. M. Liu, R. Liu and W. Chen, *Biosens. Bioelectron.*, 2013, **45**, 206–212.
43 M. Long, L. Tan, H. T. Liu, Z. He and A. D. Tang, *Biosens. Bioelectron.*, 2014, **59**, 243–250.
44 K. Yamamoto, T. Imaoka, W. J. Chun, O. Enoki, H. Katoh, M. Takenaga and A. Sonoi, *Nat. Chem.*, 2009, **1**, 397–402.
45 Y. Z. Lu and W. Chen, *J. Power Sources*, 2012, **197**, 107–110.

